Continuous-Flow Sunlight-Powered CO_2 Methanation Catalyzed by γ-Al_2O_3-Supported Plasmonic Ru Nanorods

Rohlfs, Jelle; Bossers, Koen W.; Meulendijks, Nicole; Valega Mackenzie, Fidel; Xu, Man; Verheijen, Marcel A.; Buskens, Pascal; Sastre, Francesc

DOI
10.3390/catal12020126

Publication date
2022

Document Version
Final published version

Published in
Catalysts

catalysts

MDPI

Article

Continuous-Flow Sunlight-Powered CO_2 Methanation Catalyzed by γ-Al_2O_3-Supported Plasmonic Ru Nanorods

Jelle Rohlfs [1], Koen W. Bossers [1], Nicole Meulendijks [1], Fidel Valega Mackenzie [1], Man Xu [1,2], Marcel A. Verheijen [3,4], Pascal Buskens [1,5,*] and Francesc Sastre [1,*]

1 The Netherlands Organisation for Applied Scientific Research (TNO), High Tech Campus 25, 5656AE Eindhoven, The Netherlands; jelle.rohlfs@tno.nl (J.R.); koen.bossers@tno.nl (K.W.B.); nicole.meulendijks@tno.nl (N.M.); fidel.valegamackenzie@tno.nl (F.V.M.); man.xu@tno.nl (M.X.)
2 Optics Research Group, Delft University of Technology, Lorentzweg 1 (Building 22), 2628CJ Delft, The Netherlands
3 Eurofins Materials Science, High Tech Campus 11, 5656AE Eindhoven, The Netherlands; MarcelVerheijen@eurofinsEAG.com
4 Department of Applied Physics, Eindhoven University of Technology, 5600MB Eindhoven, The Netherlands
5 Institute for Materials Research Design and Synthesis of Inorganic Materials (DESINe), Hasselt University, Agoralaan Building D, B-3590 Diepenbeek, Belgium
* Correspondence: pascal.buskens@tno.nl (P.B.); francesc.sastrecalabuig@tno.nl (F.S.)

Abstract: Plasmonic CO_2 methanation using γ-Al_2O_3-supported Ru nanorods was carried out under continuous-flow conditions without conventional heating, using mildly concentrated sunlight as the sole and sustainable energy source (AM 1.5, irradiance 5.5–14.4 kW·m^{-2} = 5.5–14.4 suns). Under 12.5 suns, a CO_2 conversion exceeding 97% was achieved with complete selectivity towards CH_4 and a stable production rate (261.9 mmol·g_{Ru}^{-1}·h^{-1}) for at least 12 h. The CH_4 production rate showed an exponential increase with increasing light intensity, suggesting that the process was mainly promoted by photothermal heating. This was confirmed by the apparent activation energy of 64.3 kJ·mol^{-1}, which is very similar to the activation energy obtained for reference experiments in dark (67.3 kJ·mol^{-1}). The flow rate influence was studied under 14.4 suns, achieving a CH_4 production plateau of 264 µmol min^{-1} (792 mmol·g_{Ru}^{-1}·h^{-1}) with a constant catalyst bed temperature of approximately 204 °C.

Keywords: carbon dioxide; Sabatier reaction; solar light; surface plasmon resonance; photochemistry

Citation: Rohlfs, J.; Bossers, K.W.; Meulendijks, N.; Valega Mackenzie, F.; Xu, M.; Verheijen, M.A.; Buskens, P.; Sastre, F. Continuous-Flow Sunlight-Powered CO_2 Methanation Catalyzed by γ-Al_2O_3-Supported Plasmonic Ru Nanorods. *Catalysts* **2022**, *12*, 126. https://doi.org/10.3390/catal12020126

Academic Editors: Son Ich Ngo and Enrique García-Bordejé

Received: 22 December 2021
Accepted: 17 January 2022
Published: 21 January 2022

1. Introduction

In the last decade, the urge to reduce greenhouse gas emissions and to close the carbon loop has led to the promotion of synthetic fuels production, using CO_2 and renewable energy as feedstock [1–3]. One of the main issues is the activation of the CO_2 molecule, which displays a high thermodynamic stability. For this purpose, several catalytic pathways have been investigated to lower the activation energy such as electrochemical, thermochemical, and photochemical/photothermal catalysis [4–6]. Direct use of sunlight to convert CO_2 into fuels and chemicals can lead to efficient systems because of the lower operating temperatures and the application of only one single energy conversion step [6–10]. Synthetic natural gas (CH_4) is an attractive product to target, as the infrastructure required for its distribution and storage is already established [11]. Additionally, it can be used as a higher energy density storage fuel compared to H_2 obtained through electrolysis. CH_4 can be produced via hydrogenation of CO_2 through the Sabatier reaction under solar light irradiation shown in Equation (1).

$$CO_2 + 4H_2 \rightarrow CH_4 + 2H_2O \; \Delta H = -165 \text{ kJmol}^{-1} \quad (1)$$

Photocatalysis aims to harvest (part of) the energy of sunlight and use it to drive chemical reactions through a coupled process where either semiconductor or plasmonic nanoparticles (NPs), or a combination of both, are used for both the interaction with the incoming photons and, subsequently, utilizing the energy of such photons to promote the catalytic conversion. Plasmonic NPs alone or supported on other materials, such as metal oxides, offer a promising approach for the CO_2 photoreduction to fuels and chemicals using sunlight due to the fact of their excellent light absorption and their unique catalytic properties [12–18]. Plasmonic NPs can harvest a particular part of the solar spectrum depending or the type of metal, shape, size, or interparticle distance [19,20]. For CO_2 photomethanation, the most common metals explored are Ni and Ru [21–33]. A literature overview on photomethanation processes is listed in Table S1. Grätzel and coworkers reported one of the first attempts of CO_2 photomethanation under mild conditions [23]. They synthetized Ru NPs supported on TiO_2 P25, which successfully produced CH_4 under simulated solar light at 1 bar, reporting an initial rate for the methane formation of 10 $\mu mol \cdot h^{-1}$ at 90 °C. Sastre et al. demonstrated CO_2 methanation with high conversion rates under solar irradiation using Ni supported on SiO_2–Al_2O_3 in a batch reactor, reporting CO_2 conversions of 94.9% with a selectivity higher than 97% for CH_4 [24]. Meng et al. reported the performance of several group VIII metals using highly concentrated light [34]. They studied the photothermal reduction of CO_2 with H_2, achieving temperatures between 350 and 400 °C. More recently, Zhang et al. reported the plasmonic behavior of Rh nanoparticles, demonstrating that light can influence not just the activity of the catalyst but also the product selectivity. They reported the selective formation of CH_4 from CO_2 for mildly illuminated reactions [35]. Under illumination, the Rh NPs show an enhanced CH_4 production rate with a high selectivity, while the CO accompanying production remains constant in comparison to dark experiments. Garcia and coworkers investigated Cu_2O nanoparticles supported on graphene, for which they reported a maximum specific CH_4 production rate of 14.93 $mmol \cdot g_{Cu2O}{}^{-1} \cdot h^{-1}$ and an apparent quantum yield of 7.84% at 250 °C [36]. Recently, our group has demonstrated that Ru nanospheres can enhance the activity towards production of CH_4 under solar light irradiation based on a collective photothermal effect [37]. Our group also demonstrated that a catalyst based on Ru nanorods (NRs) displays a remarkably broad absorption band, and that it can efficiently promote solar-powered CO_2 methanation reactions [25]. Most studies on the sunlight-powered Sabatier reaction to date, including our previous study using Ru NRs [25], were performed using batch reactors. Only a few studies report the Sabatier reaction based on plasmonic photocatalysts in a continuous-flow operation [38,39]. Garcia et al. studied the continuous-flow photo-assisted CO_2 methanation of a Ni-supported catalyst on Al_2O_3/SiO_2 for a time period of 4 h. They reported an increase of 3.7 times of the CH_4 production rate compared to the process in dark with a 3.5% CO_2 conversion under illumination at 240 $mW \cdot cm^{-2}$ and 225 °C [38]. The performance of Ru nanoparticles supported on layered double hydroxides (LDHs) has been reported for the CO_2 methanation in flow conditions by the group of Ye [39]. They achieved CO_2 conversion higher than 96% at a catalyst temperature of 350 °C under 300 W Xe lamp irradiation in 2 h experiments.

In order to scale-up and industrialize the solar-powered methanation process, more comprehensive studies aimed at understanding the effect of light intensity and flow rate on the reaction rate are required, e.g., to distinguish between photothermal and non-thermal contributions. Herein, we present a catalyst consisting of Ru NRs supported on ɣ-Al_2O_3, which successfully promoted full conversion for the CO_2 methanation with complete selectivity for CH_4 without conventional heating of the reactor and under a mild solar irradiation of up to 14.4 suns (14.4 $kW \cdot m^{-2}$). We selected this catalyst based on its broadband light absorption, which makes it capable of harvesting a large part of the solar energy, its high catalytic activity, and its ability to selectively convert CO_2 and H_2 to CH_4 [25]. Furthermore, we excluded semiconductive support materials, such as TiO_2 and CeO_{2-x}, since they can generate electron–hole pairs using the UV part of sunlight and may directly catalyze the solar methanation reaction. The impact of the solar irradiance and

flow rate on the CH_4 production rate were studied and comparative studies in dark were performed. The results indicate that the reaction process is dominated by photothermal heating of the Ru NRs. Under light conditions, the catalyst showed negligible deactivation for at least 12 h of reaction.

2. Results and Discussion

2.1. Catalyst Synthesis and Characterization

The details of the Ru-NRs/ɣ-Al_2O_3 synthesis are described in Section 3. In brief, Ru NRs were formed by thermal decomposition of $Ru_3(CO)_{12}$ deposited on ɣ-Al_2O_3 in air, followed by reduction of the formed RuO_2 nanocrystals with H_2. Thermal decomposition was performed in air at 300 °C. The resulting material, comprising RuO_2 nanocrystals, was characterized by XRD analysis (Figure S1a). The material was reduced under 5% H_2 in Ar at 250 °C (Scheme 1, see Section 3) obtaining Ru-NRs/ɣ-Al_2O_3 containing a variety of Ru nanorods and Ru nanospheres. The XRD pattern of the Ru-NRs/ɣ-Al_2O_3 (Figure 1a) showed characteristic peaks corresponding to metallic Ru and ɣ-Al_2O_3 (Figure 1a). The main diffraction peaks corresponding to metallic Ru can be observed at 38.4°, 42.1°, 44.0°, 69.4°, 78.4°, 82.2°, 84.7°, and 85.9° (ICDD 00-006-0663), while the diffraction peaks corresponding to ɣ-Al_2O_3 are shown at 31.9°, 37.6°, 39.5°, 45.7°, and 66.7° (ICDD 00-029-0063). In contrast, the XRD pattern of the ɣ-Al_2O_3 only showed peaks corresponding to ɣ-Al_2O_3 (ICDD 00-029-0063). Figure S1b shows the diffuse reflectance UV–Vis spectrum of the Ru/ɣ-Al_2O_3 catalyst, showing a broadband absorption between 350 and 850 nm in contrast to the ɣ-Al_2O_3 that displays a much higher reflectance. Thermogravimetric analysis (TGA) demonstrates that the catalyst was stable between 30 and 500 °C under N_2, and the Ru nanoparticles started oxidizing in air at 260 °C (Figure S2). The material was characterized via transmission electron microscopy (HRTEM), showing that Ru NR-like structures and nanospheres were randomly distributed on ɣ-Al_2O_3 as displayed in the high-angle annular dark field (HAADF) image in Figure 1b. The average size of the rod-like particles was 60 nm in length (Figure S1b) and 10 nm (Figure S1c) in width and 9 nm for the nanospheres (Figure S1d), determined after measuring a statistically relevant number of particles. The EDX elemental maps of Al and Ru, displayed in Figure 1g–e, confirmed the presence of Ru in the bright particles in the HAADF images. Atomic resolution TEM imaging (Figure 1h and Figure S1k) and corresponding fast Fourier transform (FFT) analysis of these images (Figure 1i and Figure S1l) confirmed the hexagonal Ru crystal structure and, thus, the metallic nature of the Ru particles. The Ru loading was analyzed through inductively coupled plasma optical emission spectroscopy (ICP-OES) analysis of the catalyst, which determined a Ru weight content of 10%. The Ru loading was not optimized to maximize the catalytic performance. Optimization of Ru loading and reaction parameters, such as temperature and pressure, will be part of future work.

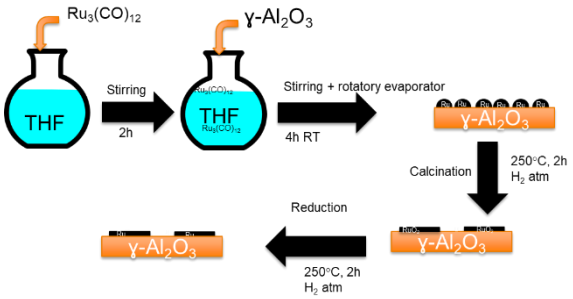

Scheme 1. Ru nanorods supported on a ɣ-Al_2O_3 preparation.

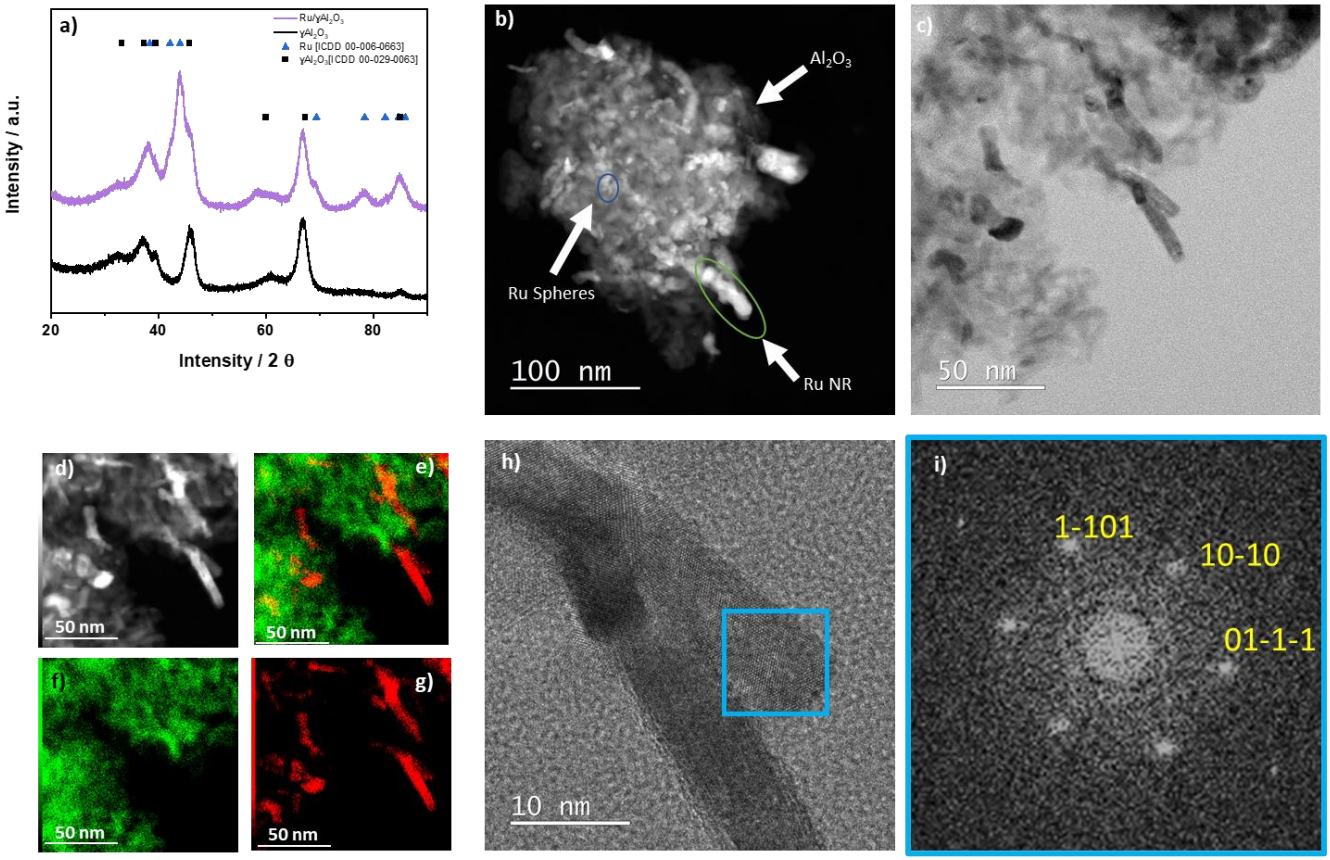

Figure 1. Structural characterization of the Ru/ɣ-Al_2O_3 catalyst: (**a**) XRD pattern of the Ru/ɣ-Al_2O_3 catalyst (purple line) and ɣ-Al_2O_3 support (black line) containing the characteristic peak positions for Ru (blue triangles, ICDD 00-006-0663) and ɣ-Al_2O_3 (black squares, ICDD 00-029-0063); (**b**) representative HAADF-STEM image of the Ru NRs and Ru nanospheres supported on ɣ-Al_2O_3; (**c**) BFTEM image of a part of a cluster showing Ru nanorods on ɣ-Al_2O_3; (**d**) HAADF-STEM of a part of the cluster shown in (**c**); (**e**–**g**) corresponding EDX elemental maps of Al (green) and Ru (red); (**h**) HRTEM image of a Ru nanorod; (**i**) FFT pattern of the area selected in (**h**), corresponding to a < 1-21-3 > zone axis pattern of the hexagonal Ru crystal structure.

2.2. CO_2 Photomethanation without Conventional Heating

The CO_2 photomethanation experiments were performed in a custom designed photoreactor system in a continuous-flow mode (Figure S3). The reactor had an opening on top with a quartz window through which artificial sunlight was irradiated on the catalyst powder bed. Prior to the experiment, 200 mg of the catalyst were loaded into the lower part of the photoreactor. Then, a mixture of H_2:CO_2:N_2 with a ratio of 4.5:1:1 was continuously led through the reactor corresponding to a flow of 9:2:2 mL·min^{-1}. N_2 was used as internal standard (see Section 3). The light source was a solar simulator (Newport Sol3A) equipped with an AM 1.5 filter and a light intensity/irradiance up to 14.4 suns (1 sun is equal to 0.1 W·cm^{-2}). The reactor temperature was monitored by a thermocouple located in the chamber ($T_{Reactor}$). The catalyst bed temperature was measured through a thermocouple placed in contact with the lower side of the catalyst bed holder ($T_{Cat\ bed}$). For the dark experiments, the reactor was heated from the bottom and laterals using electric heaters. Time zero was considered when the light was switched on, and for the dark experiments, when the desired reaction temperature was reached. Control experiments without Ru did not show any detectable product under light and dark conditions.

The performance of the Ru/ɣ-Al_2O_3 catalyst for the photomethanation of CO_2 was tested under an illumination of 12.5 suns. When the light was switched on, the CH_4 production rate increased rapidly (Figure 2a, blue line), reaching 87 μmol·min^{-1} (261.9 mmol·g_{Ru}^{-1}·h^{-1}, 97%

of conversion, after 5 min). This production rate remained constant for the 12 h time period for which we ran the reaction. The H_2 and CO_2 (Figure 2a, black and red line, respectively) decreased accordingly and remained constant until the light was switched off, resulting in a decrease of the CH_4 production rate to zero and an increase in the concentration of the reactants to their original values. The catalyst bed temperature increased rapidly after the light was switched on, reaching a spike of 222 °C and, subsequently, stabilizing at 207 °C (Figure 2b). This spike may be caused by the combination of the Ru NR acting as an efficient nanoheater under light irradiation in combination with the exothermicity of the Sabatier reaction until the reaction achieves its steady state. However, the catalyst bed temperature was stable after 30 min, and the temperature spike therefore did not have a relevant impact on the CH_4 production rate in the steady state. A detailed study on the origin of this temperature spike at the start of the process will be part of future investigations. The catalyst bed temperature was measured in the bottom part of the catalyst bed and did not correspond to the top surface temperature, as there was likely a substantial thermal gradient between the top and the bottom part of the catalyst [40–43]. This gradient was reported to exceed 100 °C for Rh/TiO_2 [44]. In contrast, the reactor temperature remained constant at 30 °C.

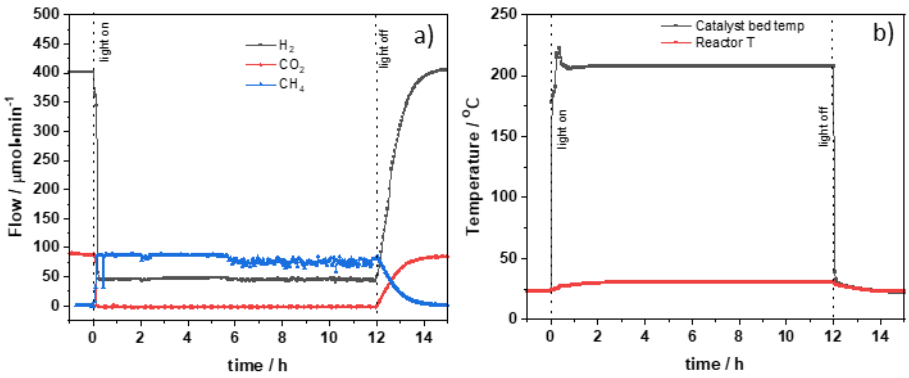

Figure 2. (**a**) CH_4 production rate as function of time for the CO_2 photomethanation without conventional reactor heating under 12.5 suns light intensity; (**b**) catalyst bed and reactor temperatures as function of time for the CO_2 photomethanation without conventional reactor heating under 12.5 suns light intensity. Reaction conditions: mixture of H_2:CO_2:N_2 (4.5:1:1) with a flow of 9:2:2 mL·min^{-1} at 1.5 bar pressure (10 wt% Ru/ɣ-Al_2O_3, 200 mg, AM 1.5 irradiance, 1 sun = 1 kW·m^{-2}).

Hot carriers, generated by the illumination of plasmonic catalyst nanoparticles, can influence the reaction in multiple ways, e.g., by injection of hot electrons into an unoccupied orbital of a nearby adsorbate (i.e., non-thermal contribution) and by increasing the catalyst's temperature (i.e., photothermal effect) [44–48]. To obtain insight into potential photothermal and non-thermal contributions, the Ru/ɣ-Al_2O_3 catalyst's performance for solar CO_2 reduction was studied under different light intensities ranging from 5.5 to 12.5 suns without conventional heating. The CH_4 production rate increased exponentially with increasing light intensity, which demonstrated the presence of a photothermal contributor (Figure 3). The CO_2 conversion increased from 1.3% under illumination of 5.5 suns to 97% under 12.5 suns illumination (Figure S4).

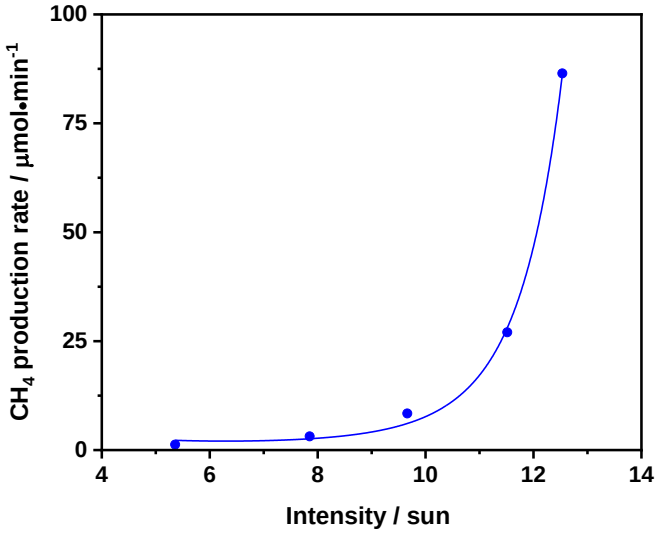

Figure 3. CH_4 production rate as function of light intensity for the CO_2 photomethanation without external heating. Reaction conditions: mixture of H_2:CO_2:N_2 (4.5:1:1) with a flow of 9:2:2 mL·min^{-1} at 1.5 bar pressure (10 wt% Ru/ɣ-Al_2O_3, 200 mg total catalyst mass, AM 1.5 irradiance (1 sun = 1 kW·m^{-2})).

In case of sole non-thermal contributions, a linear dependence of the CH_4 production rate on the applied light intensity would be expected, since the rate of molecular transformations is proportional to the rate of incident photons [40,47]. If the CH_4 production rate follows an exponential increase in the applied light intensity, a photothermal effect contributes to the reaction as reported previously by Baffou et al. [40]. In our case, the CH_4 production increased exponentially with the applied light intensity. Since the temperature of the catalyst is proportional to the light absorption and the rate constants of chemical reactions typically follow an Arrhenius type of temperature dependence, photothermal reactions display an exponential relationship between the reaction rate and the irradiance. Therefore, we propose that a large part of the observed activity was caused by collective photothermal heating of the Ru catalyst. This confirms the results obtained from our batch reaction study using the same Ru NR catalyst [25]. With the temperature obtained via the thermocouple in direct contact with the bottom of the catalyst bed (T_{cat}), an apparent activation energy of 64.3 kJ·mol^{-1} was calculated from the CH_4 production rates at different light intensities (See Equation in the Supplementary Materials). This was similar to the activation energy obtained for the same catalyst in dark (vide infra).

The influence of the flow rate on CH_4 production was studied by increasing the total flow from 89 µmol·min^{-1} of CO_2 ultimately up to 580 µmol·min^{-1} with a constant reaction mixture of H_2:CO_2:N_2 (4.5:1:1) under 14.4 suns light intensity. As displayed in Figure 4a, the CH_4 production rate exhibited a linear increase with the CO_2 flow for low flow rates. An increase in the CO_2 flow rate from 89 to 178 µmol min^{-1} led to an increase of CH_4 production from 85 to 175 µmol min^{-1} and a CO_2 conversion of 97%. At higher flow rates, the CH_4 production rate proceeded towards a plateau value of 264 µmol min^{-1} (792 mmol·g_{Ru}^{-1}·h^{-1}), while the CO_2 conversion decreased to 45.1% due to the short CO_2–catalyst contact times. The catalyst bed temperature remained constant at approximately 204 °C with an increasing flow rate (Figure 4b), confirming that the gas flow did not significantly cool down the catalyst, which is in line with a previous report by the group of Sivan [42].

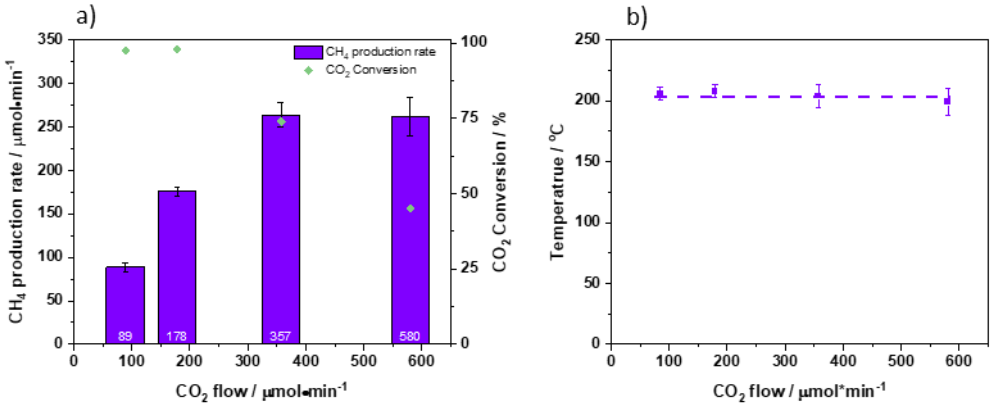

Figure 4. (**a**) CH_4 production rate as function of the reactant flow rate for the CO_2 photomethanation without conventional reactor heating under 14.4 suns light intensity without external heating; (**b**) measured temperature underneath the catalyst bed. Reaction conditions: mixture of H_2:CO_2:N_2 (4.5:1:1) at 1.5 bar pressure and 14.4 suns light intensity (10 wt% Ru/ɣ-Al_2O_3, 200 mg, AM 1.5 irradiance, 1 sun = 1 kW·m^{-2}).

2.3. Thermocatalytic CO_2 Methanation in Dark

To compare the performance under illumination to the conventional thermocatalytic process in dark, experiments in dark were performed at temperatures ranging from ambient temperature to 218 °C (Figure 5). For the experiments below 62 °C, the CH_4 formation was below the detection limit of the gas chromatograph. Based on these results, the activation energy was calculated using an Arrhenius equation, obtaining a value of 67.3 kJ·mol^{-1}. This value was similar to the apparent activation energy calculated for the light-powered reaction (64.3 kJ·mol^{-1}, vide supra), confirming that photothermal heating was the main contributor to the sunlight-powered process. Almost full CO_2 conversion was achieved at 218 °C, with a complete selectivity to CH_4.

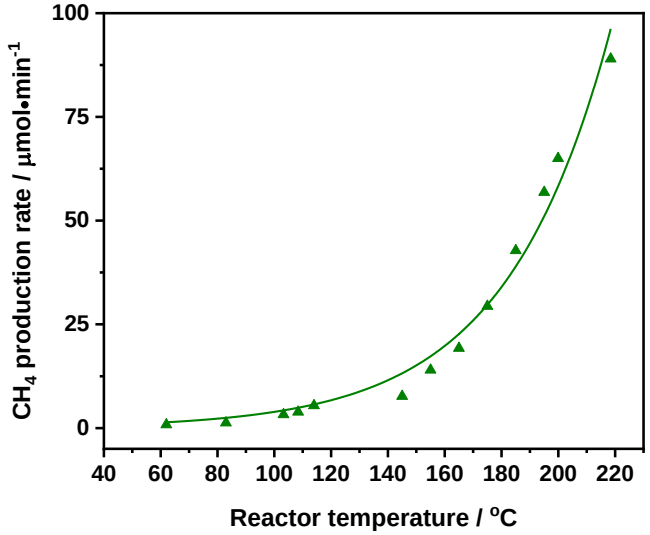

Figure 5. CH_4 production rate vs. temperature for the CO_2 methanation performed in dark. Reaction conditions: mixture of H_2:CO_2:N_2 (4.5:1:1) with a total flow of 13 mL·min^{-1} at 1.5 bar pressure (10 wt% Ru/ɣ-Al_2O_3, 200 mg total catalyst mass).

3. Materials and Methods

3.1. Synthesis of Ru Nanorods Supported on Al_2O_3

The preparation of Ru nanorods supported on ɣ-Al_2O_3 was carried out following the procedure reported previously [25]. In short, 3.2 mM Ru precursor solution was obtained by dissolving 0.32 g (0.49 mmol, 4.9 mol%) $Ru_3(CO)_{12}$ (Aldrich, St. Louis, MO, USA, 99%)

in 100 mL of THF (Biosolve, Valkenswaard, The Netherlands). The solution was stirred for approximately 2 h, until all solid was dissolved. The γ-Al_2O_3 (Alfa Aesar, 99%, S.A. 200 m^2 g^{-1}, Haverhill, MA, USA) was calcined in air at 500 °C for 6 h. Then, after cooling 1 g of calcined ɣ-Al_2O_3 was added to the precursor solution resulting in a yellow slurry. The slurry was stirred for 4 h at room temperature. Subsequently, the THF was removed in a rotary evaporator under reduced pressure at 45 °C. Calcination of the resulting composite powder was conducted in a flow of 300 mL·min^{-1} air with a heating ramp of 5 °C min^{-1} until 300 °C and at 300 °C for 2 h. The resulting material after calcination was reduced under a hydrogen flow (5% H_2 in Ar, 300 mL min^{-1}) with a heating ramp of 5 °C min^{-1} until 250 and at 250 °C for 2 h.

3.2. Characterization

XRD data sets were collected using a powder diffractometer (Panalytical, Almelo, The Netherlands) using a Prefix Bragg Brentano mirror and a HD Cu radiation source with a fixed slit of $\frac{1}{4}$ inch. A PIXcel^{1d} detector was used. An anti-scatter slit of 1 inch was used. The incident beam path was 4.41°, radius 240 mm. The used wavelength was K-Alpha1 (1.5405980 Å). Powder samples were spread on a thin layer of grease on a glass plate.

A UV–Visible diffuse reflectance spectrum was obtained using a Shimadzu UV-3600 spectrophotometer (Shimadzu, Kioto, Japan). The powder samples were pressed on a support, and their reflectance was measured in the range between 300 and 850 nm through an integrating sphere. The baseline for the measurements was determined using $BaSO_4$.

The Ru content in the catalyst was analyzed via inductively coupled plasma optical emission spectroscopy (ICP-OES) in the axial detection mode. Hereto, the sample was digested using a 10 mL mixture of mineral acids (HCl:HNO_3:HF in a 3:1:1 ratio) in a Milestone microwave setup, where upon dilution in a 50 mL polypropylene flask was carried out. The digestion procedure was executed in duplo and average values are reported. An external calibration was used for quantification starting from a 1000 ppm Perkin Elmer Ru standard in 10% HCl, and 5 ppm QC measurements were regularly checked to assure the instruments' constant performance.

Transmission electron microscopy (TEM) studies were performed using a JEOL ARM 200F transmission electron microscope (JEOL, Tokyo, Japan), probe corrected, equipped with a 100 mm^2 Centurio SDD EDX detector (JEOL, Tokyo, Japan), operated at 200 kV. Imaging was performed in the HAADF scanning TEM mode. The HAADF detector uses electrons scattered over large angles for imaging. The HAADF detector is therefore mass sensitive, which means that higher brightness in the image corresponds to the presence of (a larger concentration of) heavier atoms. This allows for a fast and accurate inventory of the Ru particle size on the ɣ-Al_2O_3 support. Samples were prepared by preparing a suspension of the material in ethanol and by depositing a drop of this suspension onto a carbon-coated copper TEM grid and drying at room temperature. In order to determine the average size of the Ru NPs and the particle size distribution, we measured the dimensions of 200 NPs from the corresponding TEM micrograph, using the image analysis software ImageJ.

The thermogravimetric analysis of the catalyst was carried out using the Discovery TGA 5500 from TA Instruments (Waters, Wakefield, MA, USA). The sample was put onto a platinum HT pan. The sample was placed in crucible under N_2 or air flow at a flow rate of 25 mL/min. The temperature was raised at a rate of 25 °C/min to 900 °C.

3.3. Gas-Phase Photocatalytic Experiments

The photocatalytic experiments were conducted in a homemade photoreactor with a quartz window on top in which a 200 mg catalyst sample was spread on a Quartz filter with an area of 3 cm^2. The catalyst bed temperature was measured by a thermocouple in contact with the bottom part of the catalyst bed (quartz filter). In a typical experiment, the reactor gas used was H_2 (Linde 6.0), CO_2 (Linde 4.5), and N_2 (Linde 5.0) with a ratio of H_2:CO_2:N_2 (4.5:1:1) of 9:2:2 mL·min^{-1}. For the dark experiments, the temperature was stabilized to the desired reactor temperature in the range from 25 to 220 °C using electrical heating.

During the experiment, the catalyst was irradiated from the top through the quartz window. The irradiation source was a solar light simulator (Newport Sol3A) (Newport Corporation, Irvine, CA, USA) provided with a filter of air mass coefficient 1.5 (AM 1.5), conventionally taken to 1 kW m^{-2}. Concentrated sunlight was obtained with a high flux beam concentrator (Newport 81030) (Newport Corporation, Irvine, CA, USA) up to an intensity of 14.4 suns. The moment the lamp was switched on, it was considered to be the starting time of the CO_2 photomethanation reaction. The gas products were analyzed by an on-line gas chromatograph (Compact GC Interscience) (Interscience, Breda, The Netherldands) every 3 min. The GC was equipped with three channels, 2 micro TCD detectors, and one FID detector. The first channel, used to measure H_2, O_2, N_2, and CO, was equipped with a MolSieve 5 Å column and RT-Q bond precolumn and TCD detector. The second channel measured CO_2, and it was equipped with a combination of a TR-U bond column and an RT-Q bond column and TCD detector. The third channel, used to measure methane, ethane, ethylene, and propane, was fitted with a Rtx-1, 2u column, and an FID detector.

Blank experiments in the presence of the catalyst at 220 °C or under illumination and in the absence of CO_2 showed no reaction products, confirming that the CH_4 originated from CO_2. In addition, no activity was observed in the absence of H_2 or catalyst.

4. Conclusions

The present study demonstrated that Ru-catalyzed sunlight-powered CO_2 methanation can be successfully performed in a continuous-flow mode with high yield and selectivity, without conventional heating, with a production rate of 87 μmol·min^{-1} (261.9 mmol·g_{Ru}^{-1}·h^{-1}, 97% of conversion, after 5 min) at 12.5 suns irradiance and a resulting catalyst bed temperature of 207 °C. This production rate remained constant for the 12 h time period, demonstrating the stability of the catalyst in use. Based on the exponential increase in the CH_4 production rate with increasing light intensity, and the similar activation energy obtained for the reaction under illumination and in dark, we conclude that photothermal heating was the main contributor to the sunlight-powered Sabatier reaction catalyzed by γ-Al_2O_3-supported Ru nanorods. This confirms the results obtained from our batch reaction study using the same Ru NR catalyst [25]. Furthermore, we demonstrated that for low CO_2 flow rates, the reaction rate of the illuminated process increased linearly with the CO_2 flow. At higher flow rates, the reaction rate proceeds towards a CH_4 production rate of 264 μmol min^{-1} (792 mmol·g_{Ru}^{-1}·h^{-1}), reaching a plateau value. At higher flow rates, the CO_2 conversion decreased from 97% to 45.1% due to the short CO_2–catalyst contact times.

Supplementary Materials: The following supporting information can be downloaded at https://www.mdpi.com/article/10.3390/catal12020126/s1, Figure S1: Optical and structural characterization of the Ru/ɣ-Al2O3 catalyst; Figure S2. Thermogravimetric analysis for Ru/ɣ-Al2O3 under N2 or air atmosphere; Figure S3. Schematic representation of the photoreactor; Figure S4. CH4 production rate and CO_2 conversion as function of light intensity for the CO_2 photomethanation without external heating; Table S1. Photocatalytic CH_4 production and reaction conditions.

Author Contributions: Conceptualization, N.M., P.B. and F.S.; methodology, K.W.B., N.M., P.B. and F.S.; software, F.V.M., M.X., K.W.B., N.M., P.B. and F.S.; validation J.R., K.W.B., F.V.M. and F.S.; formal analysis, J.R., F.V.M., M.X., K.W.B., N.M., M.A.V., P.B. and F.S.; investigation, J.R., K.W.B., F.V.M., M.A.V. and F.S.; resources, J.R., F.V.M., M.X., K.W.B., M.X., N.M., P.B. and F.S. data curation, J.R., F.V.M., K.W.B., M.X., N.M., M.A.V., P.B. and F.S.; writing—original draft preparation, K.W.B., N.M., P.B. and F.S.; writing—review and editing, J.R., F.V.M., K.W.B., M.X., N.M., M.A.V., P.B. and F.S.; visualization, N.M., P.B. and F.S.; supervision, P.B. and F.S.; project administration, N.M.; funding acquisition, N.M., P.B. and F.S. All authors have read and agreed to the published version of the manuscript.

Funding: European Fund for Regional Development through the cross-border collaborative Interreg V program Flanders, the Netherlands (project LUMEN), co-financed by the Belgian province of Limburg and the Dutch provinces of Limburg and Noord-Brabant.

Acknowledgments: J.R., K.W.B., N.M., M.X., P.B. and F.S. acknowledge the financial support from the European Fund for Regional Development through the cross-border collaborative Interreg V program Flanders, the Netherlands (project LUMEN), co-financed by the Belgian province of Limburg and the Dutch provinces of Limburg and Noord-Brabant. M.A.V. acknowledges Solliance and the Dutch province of Noord-Brabant for funding the TEM facility. We thank Wouter Marchal from Hasselt University for the ICP analyses.

Conflicts of Interest: The authors declare no conflict of interest.

References

1. Von der Assen, N.; Müller, L.J.; Steingrube, A.; Voll, P.; Bardow, A. Selecting CO_2 Sources for CO_2 Utilization by Environmental-Merit-Order Curves. *Environ. Sci. Technol.* **2016**, *50*, 1093–1101. [CrossRef] [PubMed]
2. Chen, G.; Waterhouse, G.I.N.; Shi, R.; Zhao, J.; Li, Z.; Wu, L.-Z.; Tung, C.-H.; Zhang, T. From Solar Energy to Fuels: Recent Advances in Light-driven C1 Chemistry. *Angew. Chem. Int. Ed.* **2019**, *58*, 17528–17551. [CrossRef]
3. Roy, S.C.; Varghese, O.K.; Paulose, M.; Grimes, C.A. Toward solar fuels: Photocatalytic conversion of carbon dioxide to hydrocarbons. *ACS Nano* **2010**, *4*, 1259–1278. [CrossRef]
4. Mustafa, A.; Lougou, B.G.; Shuai, Y.; Wang, Z.; Tan, H. Current technology development for CO_2 utilization into solar fuels and chemicals: A review. *J. Energy Chem.* **2020**, *49*, 96–123. [CrossRef]
5. Xu, Y.-F.; Yang, M.-Z.; Chen, H.-Y.; Liao, J.-F.; Wang, X.-D.; Kuang, D.-B. Enhanced Solar-Driven Gaseous CO_2 Conversion by $CsPbBr_3$ Nanocrystal/Pd Nanosheet Schottky-Junction Photocatalyst. *ACS Appl. Energy Mater.* **2018**, *1*, 5083–5089. [CrossRef]
6. Corma, A.; Garcia, H. Photocatalytic reduction of CO_2 for fuel production: Possibilities and challenges. *J. Catal.* **2013**, *308*, 168–175. [CrossRef]
7. Palmer, C.; Saadi, F.; McFarland, E.W. Technoeconomics of Commodity Chemical Production Using Sunlight. *ACS Sustain. Chem. Eng.* **2018**, *6*, 7003–7009. [CrossRef]
8. Linic, S.; Christopher, P.; Ingram, D.B. Plasmonic-metal nanostructures for efficient conversion of solar to chemical energy. *Nat. Mater.* **2011**, *10*, 911–921. [CrossRef] [PubMed]
9. Ren, X.; Cao, E.; Lin, W.; Song, Y.; Liang, W.; Wang, J. Recent advances in surface plasmon-driven catalytic reactions. *RSC Adv.* **2017**, *7*, 31189–31203. [CrossRef]
10. Rodriguez-Padron, D.; Luque, R.; Munoz-Batista, M.J. Waste-derived Materials: Opportunities in Photocatalysis. *Top. Curr. Chem.* **2019**, *378*, 3. [CrossRef] [PubMed]
11. Van der Zwaan, B.; Detz, R.; Meulendijks, N.; Buskens, P. Renewable natural gas as climate-neutral energy carrier? *Fuel* **2022**, *311*, 122547. [CrossRef]
12. Molina, P.M.; Meulendijks, N.; Xu, M.; Verheijen, M.A.; Hartog, T.; Buskens, P.; Sastre, F. Low Temperature Sunlight-Powered Reduction of CO_2 to CO Using a Plasmonic Au/TiO_2 Nanocatalyst. *ChemCatChem* **2021**, *13*, 4507–4513. [CrossRef]
13. Li, S.; Miao, P.; Zhang, Y.; Wu, J.; Zhang, B.; Du, Y.; Han, X.; Sun, J.; Xu, P. Recent Advances in Plasmonic Nanostructures for Enhanced Photocatalysis and Electrocatalysis. *Adv. Mater.* **2021**, *33*, e2000086. [CrossRef]
14. García-García, I.; Lovell, E.C.; Wong, R.J.; Barrio, V.L.; Scott, J.; Cambra, J.F.; Amal, R. Silver-Based Plasmonic Catalysts for Carbon Dioxide Reduction. *ACS Sustain. Chem. Eng.* **2020**, *8*, 1879–1887. [CrossRef]
15. Naldoni, A.; Riboni, F.; Guler, U.; Boltasseva, A.; Shalaev, V.M.; Kildishev, A.V. Solar-Powered Plasmon-Enhanced Heterogeneous Catalysis. *Nanophotonics* **2016**, *5*, 112–133. [CrossRef]
16. Robatjazi, H.; Zhao, H.; Swearer, D.F.; Hogan, N.J.; Zhou, L.; Alabastri, A.; McClain, M.J.; Nordlander, P.; Halas, N.J. Plasmon-induced selective carbon dioxide conversion on earth-abundant aluminum-cuprous oxide antenna-reactor nanoparticles. *Nat. Commun.* **2017**, *8*, 27. [CrossRef] [PubMed]
17. Gellé, A.; Moores, A. Plasmonic nanoparticles: Photocatalysts with a bright future. *Curr. Opin. Green Sustain. Chem.* **2019**, *15*, 60–66. [CrossRef]
18. Sastre, F.; Oteri, M.; Corma, A.; García, H. Photocatalytic water gas shift using visible or simulated solar light for the efficient, room-temperature hydrogen generation. *Energy Environ. Sci.* **2013**, *6*, 2211–2215. [CrossRef]
19. Cole, J.R.; Halas, N.J. Optimized plasmonic nanoparticle distributions for solar spectrum harvesting. *Appl. Phys. Lett.* **2006**, *89*, 153120. [CrossRef]
20. Baffou, G.; Quidant, R. Nanoplasmonics for chemistry. *Chem. Soc. Rev.* **2014**, *43*, 3898–3907. [CrossRef] [PubMed]
21. O'Brien, P.G.; Ghuman, K.K.; Jelle, A.A.; Sandhel, A.; Wood, T.E.; Loh, J.Y.Y.; Jia, J.; Perovic, D.; Singh, C.V.; Kherani, N.P.; et al. Enhanced photothermal reduction of gaseous CO2 over silicon photonic crystal supported ruthenium at ambient temperature. *Energy Environ. Sci.* **2018**, *11*, 3443–3451. [CrossRef]
22. O'Brien, P.G.; Sandhel, A.; Wood, T.E.; Jelle, A.A.; Hoch, L.B.; Perovic, D.D.; Mims, C.A.; Ozin, G.A. Photomethanation of Gaseous CO_2 over Ru/Silicon Nanowire Catalysts with Visible and Near-Infrared Photons. *Adv. Sci.* **2014**, *1*, 1400001. [CrossRef]
23. Thampi, K.R.; Kiwi, J.; Grätzel, M. Methanation and photo-methanation of carbon dioxide at room temperature and atmospheric pressure. *Nature* **1987**, *327*, 506–508. [CrossRef]
24. Sastre, F.; Puga, A.V.; Liu, L.; Corma, A.; García, H. Complete Photocatalytic Reduction of CO_2 to Methane by H_2 under Solar Light Irradiation. *JACS* **2014**, *136*, 6798–6801. [CrossRef] [PubMed]

25. Sastre, F.; Versluis, C.; Meulendijks, N.; Rodríguez-Fernández, J.; Sweelssen, J.; Elen, K.; van Bael, M.K.; den Hartog, T.; Verheijen, M.A.; Buskens, P. Sunlight-Fueled, Low-Temperature Ru-Catalyzed Conversion of CO_2 and H_2 to CH_4 with a High Photon-to-Methane Efficiency. *ACS Omega* **2019**, *4*, 7369–7377. [CrossRef]
26. Albero, J.; Garcia, H.; Corma, A. Temperature Dependence of Solar Light Assisted CO_2 Reduction on Ni Based Photocatalyst. *Top. Catal.* **2016**, *59*, 787–791. [CrossRef]
27. Yan, X.; Sun, W.; Fan, L.; Duchesne, P.N.; Wang, W.; Kubel, C.; Wang, D.; Kumar, S.G.H.; Li, Y.F.; Tavasoli, A.; et al. Nickel@Siloxene catalytic nanosheets for high-performance CO_2 methanation. *Nat. Commun.* **2019**, *10*, 2608. [CrossRef] [PubMed]
28. Melsheimer, J.; Guo, W.; Ziegler, D.; Wesemann, M.; Schlögl, R. Methanation of carbon dioxide over Ru/Titania at room temperature: Explorations for a photoassisted catalytic reaction. *Catal. Lett.* **1991**, *11*, 157–168. [CrossRef]
29. Mateo, D.; Albero, J.; García, H. Graphene supported NiO/Ni nanoparticles as efficient photocatalyst for gas phase CO_2 reduction with hydrogen. *Appl. Catal. B Environ.* **2018**, *224*, 563–571. [CrossRef]
30. Sastre, F.; Corma, A.; García, H. Visible-Light Photocatalytic Conversion of Carbon Monoxide to Methane by Nickel(II) Oxide. *Angew. Chem. Int. Ed.* **2013**, *52*, 12983–12987. [CrossRef]
31. Barrio, J.; Mateo, D.; Albero, J.; García, H.; Shalom, M. A Heterogeneous Carbon Nitride–Nickel Photocatalyst for Efficient Low-Temperature CO_2 Methanation. *Adv. Energy Mater.* **2019**, *9*, 1902738. [CrossRef]
32. Mateo, D.; Albero, J.; García, H. Titanium-Perovskite-Supported RuO_2 Nanoparticles for Photocatalytic CO_2 Methanation. *Joule* **2019**, *3*, 1949–1962. [CrossRef]
33. Steeves, T.M.; Esser-Kahn, A.P. Demonstration of the photothermal catalysis of the Sabatier reaction using nickel nanoparticles and solar spectrum light. *RSC Adv.* **2021**, *11*, 8394–8397. [CrossRef]
34. Meng, X.; Wang, T.; Liu, L.; Ouyang, S.; Li, P.; Hu, H.; Kako, T.; Iwai, H.; Tanaka, A.; Ye, J. Photothermal Conversion of CO_2 into CH_4 with H_2 over Group VIII Nanocatalysts: An Alternative Approach for Solar Fuel Production. *Angew. Chem. Int. Ed.* **2014**, *53*, 11478–11482. [CrossRef] [PubMed]
35. Zhang, X.; Li, X.; Zhang, D.; Su, N.Q.; Yang, W.; Everitt, H.O.; Liu, J. Product selectivity in plasmonic photocatalysis for carbon dioxide hydrogenation. *Nat. Commun.* **2017**, *8*, 14542. [CrossRef]
36. Mateo, D.; Albero, J.; García, H. Photoassisted methanation using Cu_2O nanoparticles supported on graphene as a photocatalyst. *Energy Environ. Sci.* **2017**, *10*, 2392–2400. [CrossRef]
37. Grote, R.; Habets, R.; Rohlfs, J.; Sastre, F.; Meulendijks, N.; Xu, M.; Verheijen, M.; Elen, K.; Hardy, A.; van Bael, M.; et al. Collective photothermal effect of Al_2O_3-supported spheroidalplasmonic Ru nanoparticle catalysts in the sunlight-powered Sabatier reaction. *ChemCatChem* **2020**, *12*, 5618–5622. [CrossRef]
38. Albero, J.; Dominguez, E.; Corma, A.; García, H. Continuous flow photoassisted CO_2 methanation. *Sustain. Energy Fuels* **2017**, *1*, 1303–1307. [CrossRef]
39. Ren, J.; Ouyang, S.; Xu, H.; Meng, X.; Wang, T.; Wang, D.; Ye, J. Targeting Activation of CO_2 and H_2 over Ru-Loaded Ultrathin Layered Double Hydroxides to Achieve Efficient Photothermal CO_2 Methanation in Flow-Type System. *Adv. Energy Mater.* **2017**, *7*, 1601657. [CrossRef]
40. Baffou, G.; Bordacchini, I.; Baldi, A.; Quidant, R. Simple experimental procedures to distinguish photothermal from hot-carrier processes in plasmonics. *Light Sci. Appl.* **2020**, *9*, 108. [CrossRef]
41. Un, I.-W.; Sivan, Y. The Role of Heat Generation and Fluid Flow in Plasmon-Enhanced Reduction–Oxidation Reactions. *ACS Photonics* **2021**, *8*, 1183–1190. [CrossRef]
42. Dubi, Y.; Un, I.W.; Sivan, Y. Thermal effects—An alternative mechanism for plasmon-assisted photocatalysis. *Chem. Sci.* **2020**, *11*, 5017–5027. [CrossRef]
43. Un, I.-W.; Sivan, Y. Thermal effect in plasmon assisted photocatalyst: A parametric study. In *Novel Optical Materials and Applications, Proceedings OSA Advanced Photonics Congress (AP) 2020 (IPR, NP, NOMA, Networks, PVLED, PSC, SPPCom, SOF), Washington, DC, USA, 13–16 July 2020*; Optical Society of America: Washington, DC, USA, 2020; p. NoTh3C.3.
44. Zhou, L.; Swearer, D.F.; Zhang, C.; Robatjazi, H.; Zhao, H.; Henderson, L.; Dong, L.; Christopher, P.; Carter, E.A.; Nordlander, P.; et al. Quantifying hot carrier and thermal contributions in plasmonic photocatalysis. *Science* **2018**, *362*, 69–72. [CrossRef] [PubMed]
45. Scaiano, J.C.; Stamplecoskie, K. Can Surface Plasmon Fields Provide a New Way to Photosensitize Organic Photoreactions? From Designer Nanoparticles to Custom Applications. *J. Phys. Chem. Lett.* **2013**, *4*, 1177–1187. [CrossRef] [PubMed]
46. Sarhan, R.M.; Koopman, W.; Schuetz, R.; Schmid, T.; Liebig, F.; Koetz, J.; Bargheer, M. The importance of plasmonic heating for the plasmon-driven photodimerization of 4-nitrothiophenol. *Sci. Rep.* **2019**, *9*, 3060. [CrossRef] [PubMed]
47. Kamarudheen, R.; Aalbers, G.J.W.; Hamans, R.F.; Kamp, L.P.J.; Baldi, A. Distinguishing Among All Possible Activation Mechanisms of a Plasmon-Driven Chemical Reaction. *ACS Energy Lett.* **2020**, *5*, 2605–2613. [CrossRef]
48. Kamarudheen, R.; Castellanos, G.W.; Kamp, L.P.J.; Clercx, H.J.H.; Baldi, A. Quantifying Photothermal and Hot Charge Carrier Effects in Plasmon-Driven Nanoparticle Syntheses. *ACS Nano* **2018**, *12*, 8447–8455. [CrossRef]